Symplectic time-domain finite element method (STD-FEM) extended with wave propagation in porous materials for automotive interior acoustic modeling

Csaba Huszty[1]*, Gergely Firtha[2], Ferenc Izsák [3]

[1]ENTEL Engineering Research & Consulting Ltd., H-1025 Budapest, Szépvölgyi út 32., Hungary

[2]Department of Networked Systems and Services, Faculty of Electric Engineering,
Budapest University of Technology and Economics, Műegyetem rkp. 3., H-1111 Budapest, Hungary

[3]Department of Applied Analysis and Computational Mathematics, Eötvös Loránd University,
H-1117 Budapest, Pázmány P. stny. 1.C, Hungary

*Corresponding author, e-mail: huszty.csaba@entel.hu

Abstract

The prediction of sound field evolving inside automotive interiors has gained significant attention in recent years, both for acoustic design purposes and virtual reality applications. Recently, a novel numerical simulation method was proposed by the present authors termed as symplectic time-domain finite element method. This paper discusses the numerical method and its application for simulating sound fields inside vehicle interiors. The presented case study includes the effect of seat absorption and non-rigid boundaries by applying either locally reacting, or elastic surface models exhibiting extended reactivity.

Keywords:
STD-FEM, time domain simulation, finite element method, absorption coefficient, admittance estimation, automotive interior acoustics

1. Introduction

The prediction of the sound field evolving in vehicles' interior have been gaining increasing interest in the recent years in the automotive industry. The topic is particularly relevant in the aspect of advanced VR applications and the computer aided acoustic design, and acoustic control of the interior sound field generated by the loudspeaker system of the cabin and external noise sources [1–3].

The numerical estimation of the interior sound field is usually performed in the angular frequency domain in the frequency band of interest, by using frequency domain finite element and—more often—by boundary element methods (FEM and BEM). In these cases special attention has to be given to calculations near resonance frequencies of the cavity (i.e. the vehicle interior). This problem is, however, completely avoided when time domain simulation methods are applied.

Recently the authors introduced a symplectic temporal finite element formulation (STD-FEM) for the solution of the 3D wave equation at arbitrary closed enclosures [9]. In the present contribution this method is applied in order to estimate the sound field inside the interior of a Skoda Octavia vehicle. The third-order temporal FEM calculation is performed on a 3D mesh of the vehicle's interior containing 176 000 tetrahedra. In order to model the interior as realistic as possible, the acoustic properties of the covering materials of the enclosure were measured with a Microflown PU-probe. From the measured absorption proper-

ties admittance-type boundary conditions were generated by applying a iterative numerical method, introduced by the authors in a recent publication [11].

The central focus of this article is to validate the finite element method by comparing it with real measurement data. This validation is demonstrated using the example of analyzing the sound field within the interior of a vehicle. To ensure precise modeling, we estimated the acoustic characteristics of various interior materials by leveraging Microflown measurements. The impulse response within the cabin was recorded and will serve as a reference point for comparing it with the numerical simulation results. Since the numerical simulations were still in progress at the time of manuscript submission, and as a result, the actual comparison results will be presented during the conference talk.

The paper is organized as follows: Section 2 provides a brief introduction to the simplectic time domain Finite Element Method (FEM), which is utilized for numerical simulations in subsequent sections. Section 3 addresses the verification of the FEM methodology. This section explores how the boundary admittances of the vehicle's interior were determined through absorption measurements, which are then employed as boundary conditions in the numerical calculations. Additionally, this section presents the vehicle model and mesh used for numerical simulations, along with the reference impulse responses recorded within the vehicle interior. The article is concluded with a concise summary.

2. Formulation of the STD-FEM

The standard model of the acoustic wave propagation is the second-order PDE

$$\partial_{tt} p(t, \mathbf{x}) = c^2 \Delta p(t, \mathbf{x}) \quad t \in (0, T), \ \mathbf{x} \in \Omega \qquad (1)$$

where $p : \Omega \to \mathbb{R}$ denotes the acoustic pressure and Ω is the computational domain. Additionally, we have to specify initial and boundary conditions.

Using Neumann boundary data for p, the weak form

$$\int_\Omega \partial_{tt} p \ v = -c^2 \int_\Omega \nabla p \cdot \nabla v + \int_{\partial\Omega} \partial_{\boldsymbol\nu} p \ v \ \forall v \in L_2(\Omega).$$

of (1) will be investigated.

For the spatial discretization of this, we define a finite element (FE) space V_h with basis $\{b_j\}_{j=1}^N$ to approximate

$$p(t, \mathbf{x}) \approx \sum_{j=1}^N p_j(t) b_j(\mathbf{x}), \quad \partial_{\boldsymbol\nu} p(t, \mathbf{x}) \approx \sum_{j=1}^{N_\mathcal{N}} p_j(t) b_j(\mathbf{x}).$$

Choosing here $v = b_k, \quad k = 1, 2, \ldots, N$, we obtain

$$\sum_{j=1}^N \partial_{tt} p_j \int_\Omega b_j \ b_k = -c^2 \sum_{j=1}^N p_j \int_\Omega \nabla b_j \cdot \nabla b_k$$
$$+ \sum_{j=1}^{N_\mathcal{N}} p_j \int_{\partial\Omega} b_j \ \partial_{\boldsymbol\nu} b_k$$

Taking it componentwise, we have the matrix vector form

$$W \cdot \partial_{tt} \mathbf{p} = S\mathbf{p} + W_b\mathbf{p}, \qquad (2)$$

where $W[j,k] = \int_\Omega b_j b_k$, $W_b[j,k] = \int_{\partial\Omega} b_j b_k$ and $S[j,k] = -c^2 \int_\Omega \nabla b_j \nabla b_k$ define the matrices of size $N \times N$ above.

To incorporate boundary conditions, we use the density $\rho_0 = 1.205$ of the air to have

$$\partial_{\boldsymbol\nu} p(t, \mathbf{x}) = \boldsymbol\nu \cdot \nabla p(t, \mathbf{x}) = -\rho_0 \partial_t \boldsymbol\nu \cdot \mathbf{v}(t, \mathbf{x}) \qquad (3)$$

In the framework of a frequency-dependent model, the response of the surface is given by the equality

$$\boldsymbol\nu \cdot \mathbf{v}(t, \mathbf{x}) = \int_0^\infty a(t_0, \mathbf{x}) \cdot p(t - t_0, \mathbf{x}) \, \mathrm{d}t_0 \qquad (4)$$

with $a(\tau, \mathbf{x})$ termed as the admittance response of the surface. In the present framework the above integral is directly discretized by sampling the admittance function as $a(t_0, \mathbf{x}) = a_1(\mathbf{x}), a_2(\mathbf{x}), ..., a_N(\mathbf{x})$ leading to the discrete form of the boundary conditions

$$\boldsymbol\nu \cdot \mathbf{v}(t, \mathbf{x}) = a_0(\mathbf{x}) \cdot p(t, \mathbf{x}) + \cdots + a_N(\mathbf{x}) \cdot p(t - N\tau, \mathbf{x}), \ (5)$$

which can be inserted into (3) to get

$$\partial_{\boldsymbol\nu} p(t, \mathbf{x}) = -\rho_0 (a_0(\mathbf{x}) \cdot \partial_t p(t, \mathbf{x}) + \ldots$$
$$+ a_N(\mathbf{x}) \cdot \partial_t p(t - N\tau, \mathbf{x})). \qquad (6)$$

Also, the coefficients $a_0, a_1, \ldots, a_N$ depend also on the delay term τ. These will be computed with a subroutine, using the inputs: N, τ and the kind of the material on the boundary. Introducing the matrices

$$L = W^{-1} S \qquad \text{and} \qquad M = \rho_0 \cdot a_0 W^{-1} Q W_b,$$

and the boundary conditions in (5), the equation in (2) can be rewritten as

$$\partial_t \begin{pmatrix} \mathbf{p}(t) \\ \mathbf{w}(t) \end{pmatrix} = \begin{pmatrix} \mathbf{w}(t) \\ L\mathbf{p}(t) + M\tilde{\mathbf{w}}(t) \end{pmatrix}, \qquad (7)$$

where the discrete delay term

$$\tilde{\mathbf{w}}(t) = \mathbf{a}_0 * \mathbf{w}(t) + \mathbf{a}_1 * \mathbf{w}(t-\tau) + \cdots + \mathbf{a}_N * \mathbf{w}(t - N\tau)$$

was applied. For the time discretization, we also need its iterated version

$$\tilde{\tilde{\mathbf{w}}}(t) = \mathbf{a}_0 * \tilde{\mathbf{w}}(t) + \mathbf{a}_1 * \tilde{\mathbf{w}}(t-\tau) + \cdots + \mathbf{a}_N * \tilde{\mathbf{w}}(t - N\tau)$$

and the following quantity

$$\tilde{\mathbf{p}}(t) = \mathbf{a}_0 * \mathbf{p}(t) + \mathbf{a}_1 * \mathbf{p}(t-\tau) + \cdots + \mathbf{a}_N * \mathbf{p}(t - N\tau),$$

where the operation $*$ yields pointwise multiplication. Similarly, can define the terms $\tilde{\tilde{\mathbf{w}}}$ and $\widetilde{L\mathbf{p}}$.

With these, we used the following time discretization of (7)

(f-i) We start from the vectors $\mathbf{p}^n$ and $\mathbf{w}^n$,

(f-ii) $\mathbf{p}_1^n = \mathbf{p}^n + \delta t \cdot \frac{1}{4} \mathbf{w}^n$,

(f-iii) $\mathbf{w}_1^n = \mathbf{w}^n + \delta t \cdot \frac{2}{3} (L\mathbf{p}_1^n + M\tilde{\mathbf{w}}^n)$,

(f-iv) $\mathbf{p}^{n+1} = \mathbf{p}_1^n + \delta t \cdot \frac{3}{4} \mathbf{w}_1^n$
$\quad + (\delta t)^3 \cdot \frac{1}{24} (L\mathbf{w}_1^n + 4M(\widetilde{L\mathbf{p}_1^n} + M\tilde{\tilde{\mathbf{w}}}^n))$,

(f-v) $\mathbf{w}^{n+1} = \mathbf{w}_1^n + \delta t \cdot (\frac{1}{3} \cdot L\mathbf{p}^{n+1} + \frac{1}{3} \cdot M\tilde{\mathbf{w}}_1^n)$
$\quad + (\delta t)^2 \cdot \frac{5}{18} M(\widetilde{L\mathbf{p}_1^n} + M\tilde{\tilde{\mathbf{w}}}^n)$
$\quad + (\delta t)^3 \cdot (\frac{1}{6} \cdot M^2(\widetilde{\widetilde{L\mathbf{p}_1^n}} + M\tilde{\tilde{\tilde{\mathbf{w}}}}^n) + \frac{1}{24} \cdot ML\tilde{\mathbf{w}}^n)$,

which is third-order accurate.

In practice, the FE space is defined on the subdomains of a grid such that it should be globally continuous.

The key compounds of an accurate and efficient simulation are the following:

- Use an appropriate basis $\{b_j\}_{j=1}^N$ to approximate the acoustic pressure accurately.

- We need a fast numerical ODE solver, which is possibly high-order, explicit and has optimal stability properties.

Moreover, the spatial discretization also affects the requirements. Rearding this, the so-called spectral or mass-lumping elements were introduced in [4], which result in a diagonal matrix M paving the way for a really explicit solver.

The construction and the analysis of corresponding FE space for a tetrahedral mesh is highly non-trivial and was performed only in the last years in [5], and [6]. Following this, we have implemented locally second-order elements extended with four higher-order terms. Practically, we have to compute with the values on the vertices, edge-midpoints, face-midpoints and interior midpoints in each tetrahedron. The tetrahedral mesh is computed with the software GMSH; see the documentation in [7]. At the same time, such a second order spatial discretization does not give an accurate approximation.

Therefore, we have turned to a fourth order accurate cubic mesh. Here, for the unit cube, we have to use the additional grid points $\left[0, \frac{1}{2} - \frac{\sqrt{21}}{14}, \frac{1}{2}, \frac{1}{2} + \frac{\sqrt{21}}{14}, 1\right]^3$, altogehter 125 ones. These has to be transformed into all cubes and constitute the Lagrange points for the finite element basis $\{b_j\}_{j=1}^N$.

The disadvantage of using such a mesh is that a middle-size uniform cubic approximation of the computational domain (in our case, the interior of the car) can be rather inaccurate.

Regarding the time step, the basis of (f-i)–(f-v) is the simple symplectic ODE solver in [8]. If the physical system preserves acoustic energy, this will be also conserved in the consecutive time steps. Also, our approach is able to deal with the filter type boundary conditions. In the corresponding mathematical model, it results in an ODE system with boundary delay. The main benefit of this approach is the optimal stability property of the corresponding scheme.

2.1. Extension with wave propagation in porous materials

A further possible extension is to make the coefficient c to be space-dependent. In this way, the propagation of the sound within the covering materials or seats can also be taken into account. To streamline the simulations, c is usually constant within one space element. This does not harm the element-wise evaluation of the matrix S.

2.2. Performance and stability

In a previous series of experiments, we pointed out that the spatial cubic grid combined with the time stepping in (f-i)-(f-v) exhibits good approximation properties. In concerete terms, the theory in [4] ensures the fourth-order spatial approximation, moreover, the stability of (f-i)-(f-v) is optimal. Accordingly, we can use time steps corresponding to the physical time of sound propagation between the gridpoints to maximize the simulation speed in this framework. This stability property is sligthly changed in case of tetrahedral elements.
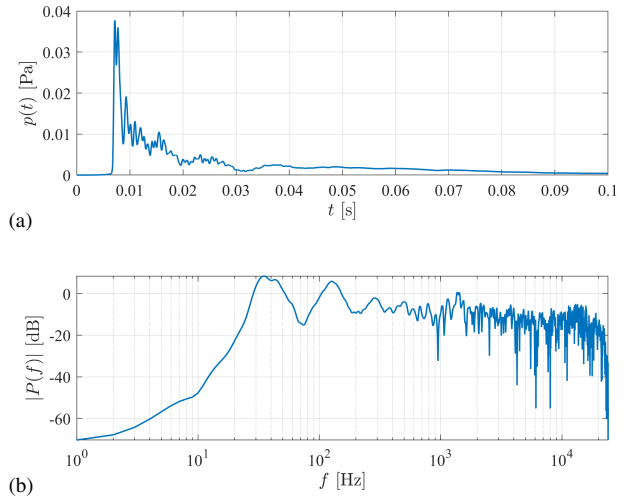

Figure 1: Envelope of the measured impulse response (a) and measured frequency response (b) in the vehicle's interior

3. Verification

The primary objective of this article is to validate the numerical methodology by comparing the simulated results with real measurement data inside an actual vehicle's interior. The simulation and the reference measurement were carried out in a small enclosure being the interior of a C-segment family car (Škoda Octavia Mk2 Typ 1Z Facelift). Regrettably, the actual comparison is not included in this article because the numerical calculations were ongoing at the time of submission. However, we intend to present these comparative results during our conference talk.

In the following sections, we discuss into the reference impulse response (IR) measurement and the prerequisites necessary for the numerical simulations. These prerequisites encompass the appropriate geometric model and the resulting mesh of the vehicle interior, as well as the estimation of surface admittance based on measurements of the interior walls.

3.1. Reference IR measurement

As a basis of comparison the impulse response between a predefined source and receiver position was captured inside the vehicle's interior.

As a sound source a Genelec 8351A was employed, excited by a wide band sine sweep in the audible frequency region. In the receiver position the sound field was captured by using an MH Acoustics Eigenmike em32 spherical microphone array, containing 32 individual microphone capsule. The spherical array allows the capture of directional impulse responses, however, in the present study only the omnidirectional signal was used as a reference measurement, obtained by averaging the individual microphone signals with equal weights. Finally, the omnidirectional impulse response was obtained by deconvolving the excitation signal from the measured response.

The results of the measurement in the temporal and fre-

quency domain is depicted in Figure 1. The temporal illustration depicts the envelope of the impulse response, calculated by the amplitude of the measured IR's Hilbert transform, with also applying temporal smoothing. These results will later serve as the reference for the comparison with simulated data.

3.2. Measurement based estimation of material properties

In order to give a reliable estimation for the impulse response by means of the numerical methodology, described in Section 1 suitable boundary conditions are required. As it is defined by (4) in the current framework the admittance of the surface points are incorporated directly into the numerical simulation. Therefore, in order to define appropriate boundary conditions, the surface admittance of the different covering materials, bounding the enclosure had to be estimated.

Boundary types:

In the current research the boundary of the enclosure was devided into 6 different categories, having different absorption properties and surface admittance. The different boundary cover categories were

- seats with porous covering

- roof of the enclosure

- door panel with fabric cover

- plastic dashboard

- trunk upholstery

- glass (e.g. windshield, windows)

Boundary surface model:

As it is reflected by (4) all the materials were considered to be locally reacting, i.e. at each surface position the surface velocity only depends on the pressure history at the same location. This assumption is a severe simplification, completely discarding wave propagation below and over the surface of the boundary, e.g. inside the porous layer of the seats. Simply saying, as a result, acoustic waves can not travel through the materials inside the enclosure.

The locally reactive assumption, however, was essential in terms of the physical feasibility of the number of measurements: in order to incorporate extenededly reactive surface models, the number of impedance/admittance measurements described in the following would be proportional with the square of the measurement positions defined above the surface of interest, leading to infeasible number of measurements at high frequencies.

Furthermore, extended reactive surface assumption would also require weighted pressure contribution from all the possible boundary positions in (4), leading also to a significant increase in the simulation computation time.

Figure 2: Measurement of surface impedance with a Microflown PU-probe

Surface admittance estimation:

With the above locally reactive surface model individual admittance frequency response had to be estimated to each of the 6 cover types. Obviously, from the admittance frequency response, temporal responses can be directly calculated by means of an inverse Fourier transform, yielding the required admittance response $a(t, \mathbf{x})$.

The admittance measurement was carried out by using a Microflown PU-probe to capture both the pressure and the normal particle velocity on the surface, when the surface was exposed to an incident wave field. The incident wave field was generated by using again, a Genelec 8351A loudspeaker, at each measurement position directed towards the microflown sensor, placed as close to the surface as it was physically possible.

Since the actual surface admittance heavily varies over the surface of cover materials even from the same category, an average admittance was estimated to each cover type. The methodology for estimating the average admittance for a single cover type was the following:

Assuming that pressure and normal velocity frequency responses, measured at the i-th measurement position are denoted as $P_i(\omega)$ and $V_i(\omega)$, the local specific impedance at the measurement position is given by

$$Z_i(\omega) = \frac{P_i(\omega)}{V_i(\omega)}. \tag{8}$$

From the estimated impedance the directional absorption coefficient at the i-th location is calculated with respect to the inclination angle of the incident wave field θ as
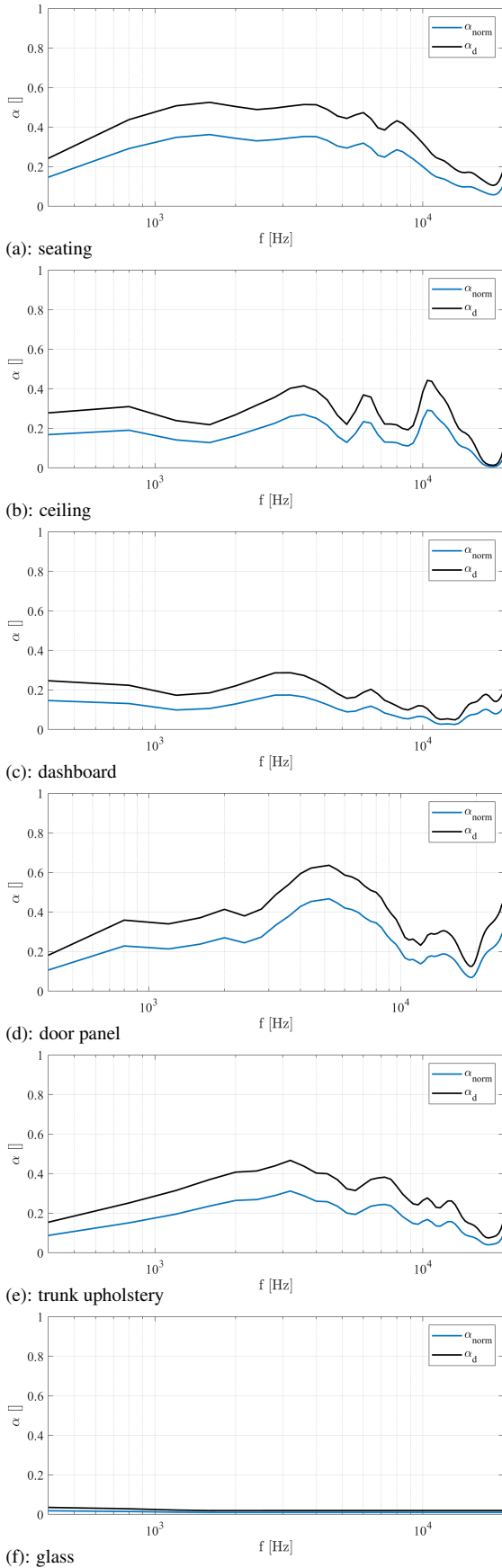
$$\alpha_i(\omega,\theta) = \frac{4\mathrm{Re}(Z_i)/\cos\theta}{\left|Z_i + 1/\cos\theta\right|^2}. \tag{9}$$

The estimated α_i absorption coefficients were minimized to zero and logarithmically smoothed in the frequency domain, denoted by α_i'. From the smoothed directional absorption data the diffuse field absorption at the i-th measurement position was calculated as

$$\alpha_{d,i}(\omega) = \frac{2}{\pi} \int_0^{\pi/2} \alpha_i'(\omega,\theta)\cos(\theta)\sin(\theta)\,\mathrm{d}\theta. \tag{10}$$

Finally, the average diffuse absorption coefficient of the cover type was calculated as the average of the individual measurement results

$$\alpha_d(\omega) = \frac{1}{I}\sum_1^I \alpha_{d,i}(\omega). \tag{11}$$

In a recent contribution by the authors of this paper [11], a novel numerical methodology was introduced. This approach enables the prediction of surface admittance responses exclusively utilizing the frequency-dependent diffuse absorption coefficient. The proposed technique reconstructs the discarded phase information (i.e. the complex admittance frequency response) relying on the causality and passivity requirements for the underlying system, being true for any physical absorber structure. By adhering to these physically motivated principles, the complex admittance response is obtained by Newton-Raphson iteration, converging typically into the minimal phase solution of the problem —i.e. obtaining the shortest, most compact possible temporal admittance response that realizes the target diffuse absorption coefficient— being a feasible feature in the aspect of using the obtained admittance response as boundary conditions in the present simulation scenario.

In the present case this numerical technique was applied in order to obtain admittance responses from the average diffuse absorption coefficient (11) for a given covering material type. Hence, instead of directly measuring an average admittance over points of a surface type by using the Microflown sensor, the average diffuse absorption factor above the measurement positions was estimated, to which a corresponding admittance response was assigned. The implemented approach was advantageous, since in case of direct admittance estimation even minor measurement errors can result in non-passive and non-causal admittance estimation.

From the obtained admittance responses, again either a diffuse or oblique incident absorption coefficient can be expressed. The diffuse and normal incidence absorption proties of the different covering types are depicted in Figure 3 (a-f). It is highlighted, that due to its physical properties, the seating behaves as a porous, wide-band absorber. On the other hand, the ceiling, the dashboard and the door panels behave more as resonant absorbers due to the cavities behind the covering materials. Finally, the glass surfaces act as almost ideal rigid boundaries.

(a): seating

(b): ceiling

(c): dashboard

(d): door panel

(e): trunk upholstery

(f): glass

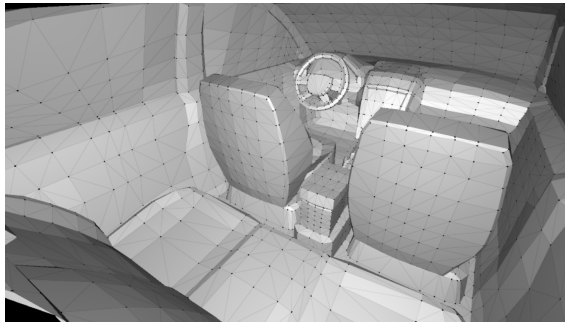Figure 3: Average diffuse and normal absorption coefficients of the interior covering materials

Figure 4: 3D model of the vehicle interior

3.3. Simulation of sound field inside the vehicle

For the implementation of the STD-FEM, a 3D model of the vehicle's interior was created. A snapshot of the model is depicted in Figure 4.

Based on the 3D model the automotive interior is tessellated into a tetrahedral mesh using the software GMSH, containing 176 000 tetrahedra. This software is flexible regarding the order and the shape of the mesh elements. In concrete terms, we could choose also hexahedral elements. As a result, we obtain a numbering of the nodes and a list with the tetrahedra containing the node numbers of its vertices, two internal edge nodes and face midpoints. To implement the second order tetrahedral element in [5], these have to be completed with the element midpoint and on the edges, we merged the nodes into the midpoint.

4. Summary and conclusions

The manuscript presented a symplectic finite element formulation, allowing the estimation of sound fields inside enclosures directly in the temporal domain. The methodology is applied for calculating the impulse response in an actual vehicle's interior.

To ensure precise simulations, a detailed tetrahedral mesh comprising 176 000 tetrahedral elements was generated for the interior of a Škoda Octavia Mk2. The interior covering surfaces were measured using a Microflown PU probe, enabling the determination of average absorption coefficients for six distinct covering materials. Through a numerical method previously proposed by the authors in a different publication, these absorption coefficients were converted into surface admittance functions. These functions will serve as boundary conditions for subsequent numerical simulations. The results from the Finite Element Method (FEM) simulations are planned for comparison with impulse responses captured within the vehicle's interior.

5. Acknowledgements

References

[1] Y. Soeta, Y. Sakamoto, *An Exploratory Analysis of Sound Field Characteristics using the Impulse Response in a Car Cabin.* Environemnts, 2018, 5(4), DOI: 10.3390/environments5040044

[2] T. Dupré, S. Denjean, M. Aramaki, R. Kronland-Martinet *Spatial Sound Design in a Car Cockpit : Challenges and Perspectives.* 2021 Immersive and 3D Audio: from Architecture to Automotive (I3DA), Sep 2021, Bologna, France. pp.1-5, 10.1109/I3DA48870.2021.9610910.hal-03456711

[3] S. Paik, M. De Geest, K. Vansant, *Interior Acoustic Simulation for In-Car Audio Design.* Sound and Vibration, Jan 2013, 47(1), Pages 10–16

[4] D. Komatitsch, J. Tromp, *Introduction to the spectral element method for three-dimensional seismic wave propagation.* Geophysical Journal International, Dec 1999, 139(3), Pages 806–822, DOI: 10.1046/j.1365-246x.1999.00967.x

[5] S. Geevers, W. A. Mulder, J. J. W. van der Vegt, *New higher-order mass-lumped tetrahedral elements for wave propagation modelling.* SIAM Journal on Scientific Computing, Jan 2018, 40(5), 2830–2857, DOI: 10.1137/18M1175549

[6] S. Geevers, W. A. Mulder, and J. J. W. van der Vegt, *Efficient quadrature rules for computing the stiffness matrices of mass-lumped tetrahedral elements for linear wave problems.* SIAM Journal on Scientific Computing, Jan 2019, 41(2), A1041–A1065, DOI: 10.1137/18M1198557

[7] C. Geuzaine, J.-F. Remacle, *GMSH: A three-dimensional finite element mesh generator with built-in pre- and post-processing facilities.* International Journal for Numerical Methods in Engineering, 2009, 79(11), 1309–1331, DOI: 10.1002/nme.2579

[8] S. Liu, D. Yang, J. Ma, *A modified symplectic PRK scheme for seismic wave modeling.* Computers & Geosciences, 2017, 99, 28–36, DOI: 10.1016/j.cageo.2016.11.001

[9] C. Huszty, F. Izsak, *Symplectic time-domain finite element method (STD-FEM) for room acoustic modeling.* InterNoise 2023, Chiba, Greater Tokyo, Japan, 20-23 August, 2023

[10] G. Firtha, C. Huszty, *Measurement Based Absorption Characteristics Estimation of Extended Reactive Surfaces.* Forum Acusticum 2023, 10th Convention of the European Acoustics Association, Politecnico di Torino, Turin, Italy, 11–15 September, 2023

[11] C. Huszty, G. Firtha, *Prediction of surface admittance impulse responses from frequency-dependent sound absorption coefficients.* InterNoise 2023, Chiba, Greater Tokyo, Japan, 20-23 August, 2023

[12] G. Firtha, C. Huszty, *A 3D modeling method of layered acoustic material structures with finite dimensions.* InterNoise 2023, Chiba, Greater Tokyo, Japan, 20-23 August, 2023